Geophysical Research Letters

RESEARCH LETTER
10.1029/2024GL111770

Key Points:

- The atmospheric response to ocean heat transport (OHT) anomalies in the western boundary currents (WBC) is examined
- Anomalous OHT drives robust changes in the atmospheric circulation and convective precipitation over the WBCs of both hemispheres
- The Northern Hemisphere responses extend to the upper troposphere; the Southern Hemisphere responses are limited to the lower troposphere

Supporting Information:

Supporting Information may be found in the online version of this article.

Correspondence to:

L. Sun,
lantao.sun@rams.colostate.edu

Citation:

Sun, L., Patrizio, C., Thompson, D. W. J., & Hurrell, J. W. (2025). Influence of anomalous ocean heat transport on the extratropical atmospheric circulation in a high-resolution slab-ocean coupled model. *Geophysical Research Letters*, *52*, e2024GL111770. https://doi.org/10.1029/2024GL111770

Received 1 AUG 2024
Accepted 27 JAN 2025

Influence of Anomalous Ocean Heat Transport on the Extratropical Atmospheric Circulation in a High-Resolution Slab-Ocean Coupled Model

Lantao Sun[1], Casey Patrizio[2], David W. J. Thompson[1,3], and James W. Hurrell[1]

[1]Department of Atmospheric Science, Colorado State University, Fort Collins, CO, USA, [2]The Euro-Mediterranean Center on Climate Change (CMCC), Bologna, Italy, [3]School of Environmental Science, University of East Anglia, Norwich, UK

Abstract Key questions remain about the atmospheric response to variability in the oceanic western boundary currents (WBCs). Here we exploit a unique high-resolution slab-ocean coupled climate model to investigate how ocean heat transport (OHT) anomalies in the major WBCs of both hemispheres affect the atmospheric circulation. Prescribed OHT anomalies lead to robust changes in convective precipitation anomalies equatorward of the maximum surface warming. The response is deepest and most pronounced over the Northern Hemisphere (NH) WBCs, where it is associated with significant changes in upper tropospheric vertical motion, condensational heating and geopotential heights. The response is relatively shallow over the Southern Hemisphere (SH) WBCs. The findings reveal the robustness of the atmospheric response to OHT anomalies and highlight key hemispheric differences: in the NH, OHT anomalies are balanced by deep atmospheric vertical motion; in the SH, they are balanced primarily by shallow horizontal temperature advection.

Plain Language Summary We study how ocean heat transport (OHT) influences the atmospheric circulation in the major western boundary currents (WBCs) of both hemispheres, including the Gulf Stream, Kuroshio-Oyashio Extension, Brazil-Malvinas Confluence, and Agulhas Currents. We find that the heating due to anomalous ocean heat transport causes air to rise on the equatorward side of the largest surface heating in all WBC regions. The regions of rising air are also associated with more intense convective precipitation. The effect is strongest in the Northern Hemisphere (NH) where the atmospheric response extends to the upper troposphere, leading to significant heating and atmospheric circulation anomalies aloft. The findings highlight the robustness of the atmospheric response to ocean dynamical processes in the western boundary currents, although differences in the hemispheric responses are noteworthy. In the NH WBCs, the atmospheric response to OHT anomalies is balanced primarily through vertical air movement, whereas in the Southern Hemisphere, the response is balanced primarily by low-level horizontal temperature advection.

1. Introduction

The ocean heat transport (OHT) in the western boundary currents (WBCs) gives rise to large exchanges of heat between the atmosphere and ocean and pronounced meridional gradients in sea-surface temperature (SST). The surface fluxes associated with the WBCs influence key aspects of the extratropical atmosphere on climatological-mean timescales, such as the distribution of precipitation and the position of the midlatitude jet (e.g., Minobe et al., 2008; Nakamura et al., 2008; O'Reilly et al., 2017). They have also been shown to influence the extra-tropical atmospheric circulation over the Gulf Stream and Kuroshio-Oyashio Extension on monthly and annual timescales. Anomalies in sea-level pressure, precipitation, vertical motion and atmospheric eddy heat transport, for example, have been linked to oceanic variability related to meridional displacements of the WBCs and the associated mesoscale oceanic eddy activity (e.g., Famooss Paolini et al., 2022; Frankignoul et al., 2011; Joyce et al., 2019; Ma, Jing, et al., 2016; Nakamura et al., 2012; Patrizio & Thompson, 2022; Siqueira & Kirtman, 2016; Smirnov et al., 2015). Despite significant improvements in our understanding of the atmospheric response to oceanic variability in the WBC regions, however, key questions remain related to the precise mechanisms, amplitude, and spatial pattern of the response (e.g., Wills et al., 2024). This is particularly true in the Southern Hemisphere (SH), where the signature of the major WBCs in the atmospheric circulation has received much less attention (Nkwinkwa Njouodo et al., 2018; Reason, 2001).

The atmospheric response to midlatitude SST anomalies is difficult to detect in observations because the surface heat fluxes associated with a typical midlatitude SST anomaly can generally be balanced by relatively small changes in lower tropospheric horizontal temperature advection. Thus, the atmospheric response to extratropical SST variability is frequently shallow and modest compared to the large internal variability in the extratropical circulation (Czaja et al., 2019; Hoskins & Karoly, 1981; Kushnir et al., 2002). It is also frequently complicated by nonlinear dynamics, which transform the linear response into a pattern that resembles the extratropical atmospheric circulation anomalies that force midlatitude SST anomalies in the first place (e.g., Deser et al., 2003; Peng & Robinson, 2001; Peng & Whitaker, 1999). This contrasts with the surface heat fluxes associated with a typical tropical SST anomaly, which are not balanced by horizontal temperature advection and are thus capable of generating a deep response in atmospheric vertical motion and condensational heating (Hoskins & Karoly, 1981).

Model experiments, often performed with prescribed SST forcings and large ensembles, have been widely used to isolate and understand how WBCs impact the atmosphere, particularly over the Gulf Stream (e.g., Famooss Paolini et al., 2022; Hand et al., 2014; Minobe et al., 2008; O'Reilly et al., 2017; Parfitt et al., 2016; Seo et al., 2017; Wills et al., 2024) and Kuroshio-Oyashio Extension (e.g., Smirnov et al., 2015; Yook et al., 2022). However, such simulations can have significant limitations, including a lack of coupled atmosphere–ocean interactions and insufficient model horizontal resolution (e.g., Small, Bryan, et al., 2019). Indeed, previous simulations run with coarse resolution ($\geq 1°$) models generally exhibit the theoretical linear response to midlatitude SST anomalies, while finer-scale ($\leq 0.25°$) simulations generally exhibit stronger responses in vertical motion and eddy heat transport that extend deeper into the troposphere, which is more consistent with observational estimates (e.g., Famooss Paolini et al., 2022; Smirnov et al., 2015; Wills et al., 2024). These studies emphasize the importance of sufficient horizontal resolution in accurately modeling the large-scale response of the atmospheric circulation to midlatitude SST anomalies.

The impact of WBCs on the atmospheric circulation has also been demonstrated by comparing high-resolution and low-resolution model output from more realistic atmosphere–ocean global climate model (AOGCM) simulations or by spatially-filtering the small-scale oceanic variability over WBC regions in model experiments. Ocean mesoscale-eddy variability has been shown to play a crucial role in enhancing atmospheric variability (e.g., Small et al., 2008) and significantly impacting jet streams, large-scale atmospheric flow and midlatitude storm tracks at subseasonal-to-seasonal timescales (e.g., Jia et al., 2019; Ma, Nakamura, et al., 2016; O'Reilly et al., 2017; Small, Msadek, et al., 2019). More recent work by Larson et al. (2024) demonstrated that the observed variability in vertical motion and precipitation across global WBCs is well simulated in a high-resolution version of a coupled climate model (0.1° ocean; 0.25° atmosphere) but poorly simulated in a low-resolution version (1° ocean and atmosphere). Overall, these studies highlight that small-scale processes associated with atmosphere–ocean interactions over WBCs are important for realistically simulating various aspects of midlatitude ocean–atmosphere variability.

Previous work has generally focused on the impacts of small-scale oceanic forcing in WBC regions on the atmospheric circulation, so in this study we explore the influence of *large-scale* ocean variability in WBC regions in both hemispheres. To do so, we conduct a series of numerical experiments run on a unique, high-resolution, slab-ocean model developed specifically for this study. There are three key aspects to the approach: (a) We force the model with reanalysis estimates of OHT rather than SST anomalies. As such, the atmospheric response can be directly attributed to ocean processes including both ocean dynamics and Ekman dynamics (e.g., Kwon et al., 2011; Sutton & Mathieu, 2002); (b) A slab-ocean coupled model has an advantage over fixed SST experiments used in many previous studies since the response to local heating can be balanced thermodynamically over remote regions of the global ocean; and (c) We compare and contrast the response to OHT anomalies over major WBC regions of both hemispheres: the Gulf Stream and Kuroshio-Oyashio Extension in the Northern Hemisphere (NH), and the Brazil-Malvinas Confluence and Agulhas current systems in the SH. As noted in the results, the atmospheric responses exhibit considerable differences from one WBC to the next.

2. Analysis Design

All simulations are based on the International Laboratory for High-Resolution Earth System Prediction (iHESP) high-resolution configuration of the Community Earth System Model Version 1.3 (CESM v1.3; Chang et al., 2020; Hurrell et al., 2013; Meehl et al., 2019; Zhang et al., 2020). The iHESP configuration features a nominal horizontal resolution of 0.25° for the atmosphere and land, and 0.1° for the ocean and sea ice models. We

developed a thermodynamic (mixed-layer) slab ocean model (iHESP-SOM) for our WBC experiments. The slab-ocean configuration is a simplified ocean model operating at every global ocean grid point, approximating the well-mixed ocean mixed layer. There is no direct communication between adjacent ocean grid points, nor any explicit representation of the deep ocean (Knutson, 2003). In the iHESP-SOM, the convergence of OHT is prescribed as a Q-flux adjustment, thus allowing for the investigation of how variations in OHT impact atmospheric circulation (e.g., Tomas et al., 2016).

The iHESP-SOM control simulation was created by applying a seasonally and spatially varying climatological mean Q-flux, along with a spatially varying but constant-in-time mixed-layer depth, to the slab-ocean model. The climatological mean Q-flux and mixed-layer depth fields used to create the control simulation were derived from the 60-year climatology of ice-ocean hindcast runs, utilizing atmospheric data from a reanalysis product with interannually varying conditions (i.e., JRA-55 do; Tsujino et al., 2018). The control simulation was run for 22 years under perpetual year-2020 radiative forcing, with the initial 2 years discarded as spin-up. The control simulation yields realistic representations of the observed climatological-mean atmospheric circulation and SST fields and does not indicate a drift in global mean temperature.

We probe the influence of variability in OHT on the atmospheric circulation over four WBC regions as follows. First, we calculate the Q-flux forcing associated with OHT variability in the major WBCs noted above. We did not perform experiments for the East Australian Current due to its relatively small Q-flux variability compared to other WBC regions. OHT variability was estimated using the indirect method from Patrizio and Thompson (2021), in which the ocean heat flux convergence ($Q_o^{'}$) is calculated as a residual term in the energy budget of the ocean mixed-layer:

$$Q_o^{'} = \rho C_p \bar{h} \frac{\partial T^{'}}{\partial t} - Q_s^{'}$$

where primes indicate monthly-mean anomalies, and the overbar represents the climatological mean over all months. ρ is the density of water and C_p is the ocean heat capacity. h is the climatological mixed-layer depth from JRA-55 (Kobayashi et al., 2015). T is the monthly-mean mixed-layer temperature, approximated by Optimum Interpolation-SST version 2.1 (OISST-v2.1; Huang et al., 2021). Q_s is the net surface heat flux from ERA-5 (Hersbach et al., 2020), encompassing the latent, sensible and net radiative fluxes at the surface. Note that the same equation was used to calculate the climatological mean Q-flux, except that climatological SSTs and surface heat fluxes from JRA-55 hindcasts were used instead of observation-based anomalies. $Q_o^{'}$ has been regridded from 0.25° to 0.1° to match the iHESP-SOM ocean grid. The linear trend was removed from the SST and surface heat flux anomalies before calculating $Q_o^{'}$.

The Q-flux patterns used to force the SOM were formed as follows. First, we generate the 1982–2022 monthly time series of OHT convergence for each WBC region by: (a) averaging values of $Q_o^{'}$ anomalies within specific WBC boundaries: 37.5–45°N, 40–72°W for the Gulf Stream; 37–44°N, 140–180°E for the Kuroshio-Oyashio Extension; 35–55°S, 15–55°W for the Brazil-Malvinas Confluence; and 35–50°S, 5–85°E for the Agulhas Current (indicated in Figure 1 by green boxes for each WBC); and (b) normalizing the resulting area-averaged time series by dividing it by its standard deviation. We then form the spatial patterns associated with variability in the WBCs by regressing the spatially varying $Q_o^{'}$ field onto the standardized WBC-mean $Q_o^{'}$ time series. The regressions were performed during the boreal and austral cold season months: that is, October-March in the NH and April-September in the SH. Finally, we multiply the resulting regression maps by two and set values outside the WBC regions to zero to generate the patterns of Q-fluxes associated with a 2σ deviation in OHT convergence within each WBC. These regression maps are then smoothed with a cosine tapered window to minimize discontinuities at the edges of the forcing patterns (e.g., see also Smirnov et al., 2015). We note that the regression maps differ from the local grid point regression applied in Larson et al. (2024) and the spatially filtered patterns in Jia et al. (2019), both of which are more strongly tied to small-scale processes. The goal of this study is to explore the impacts of the large-scale WBC variability on the atmosphere, not only the effects of mesoscale ocean processes. While small-scale variability is removed with area-averaging, a component of the larger-scale WBC variability is driven by processes operating at relatively small scales via eddy–WBC interactions (Qiu & Chen, 2010).

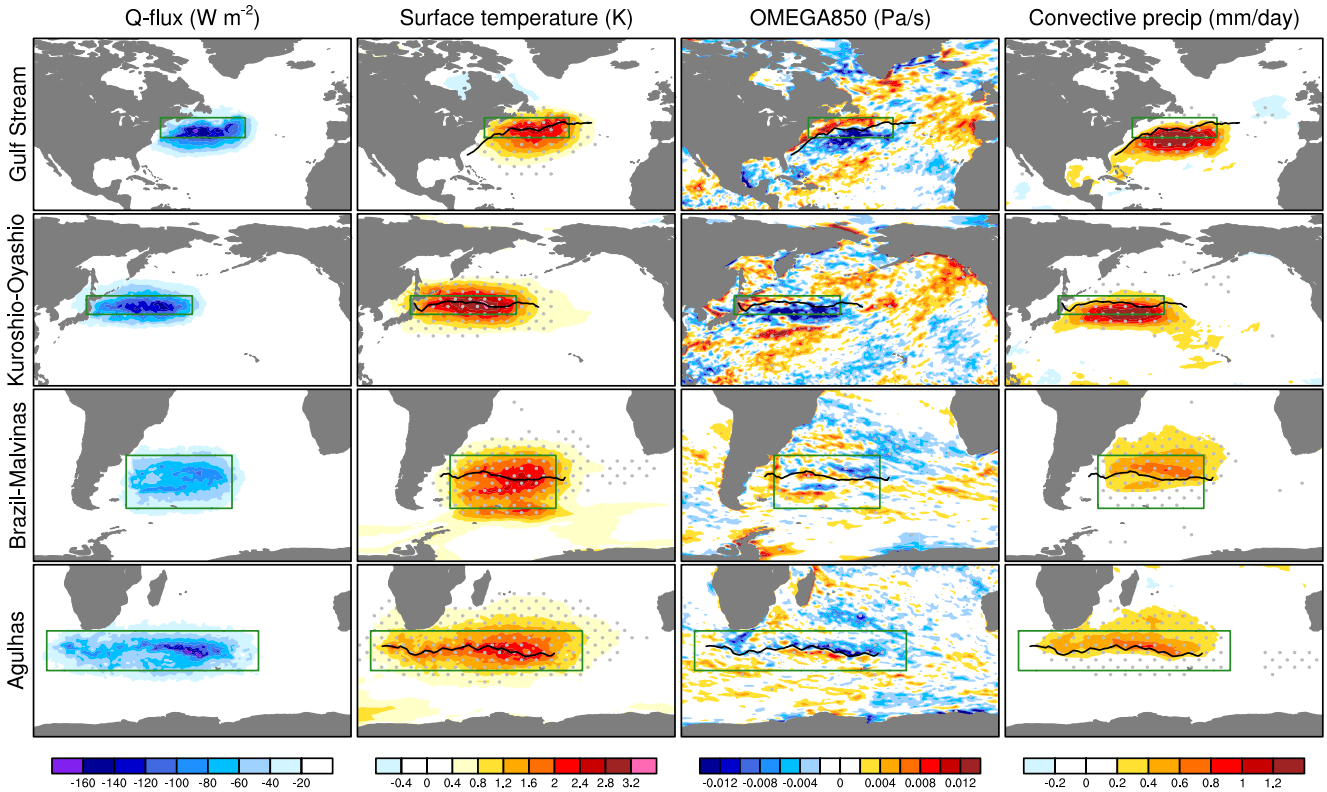

Figure 1. Q-flux forcings applied to a slab-ocean coupled climate model (left panel; unit of W m^{-2}) and the responses of surface temperature (middle left; unit of K), 850-hPa vertical motion (middle right; unit of Pa s^{-1}), convective precipitation (right panel; unit of mm day^{-1}), averaged during the extended winter months across four major western boundary currents in both hemispheres. The results correspond to the difference between the anomalies obtained in the $+2\sigma$ and -2σ perturbation experiments. Black curves highlight the latitudes with the maximum surface temperature responses. Stippled areas represent regions where results are statistically significant at the 95% level, determined by a two-sided student's *t*-test. Green boxes denote the WBC boundaries.

The resulting Q-flux (i.e., OHT convergence) forcing patterns are shown in the left row of Figure 1. The amplitudes in Figure 1 (left) correspond to the difference between a $+2\sigma$ and -2σ anomaly in OHT over the respective regions. The patterns indicate notable variations in magnitudes and geographic shapes among the four WBCs. For example, the ocean heat flux convergences in the Gulf Stream and Kuroshio-Oyashio Extension are larger than those in the Brazil-Malvinas Confluence and Agulhas; the latitudinal range for NH WBC regions spans 35°N to 45°N, whereas the SH WBC regions generally span 35°S–50°S; the Agulhas ocean current encompasses approximately 80° of longitude, nearly twice that of the other three currents; and variability in the Brazil-Malvinas Confluence current system resembles a horseshoe pattern with two maxima at the western longitudes and a single maximum on the eastern side. We note that patterns like those shown in the left column are also obtained through Empirical Orthogonal Function (EOF) analysis of the $Q_o^{'}$ field (Figure S1 in Supporting Information S1) over each WBC region, which indicates that the patterns of OHT convergence used to force our experiments also correspond to the leading patterns of OHT variability.

We conduct a series of perturbation experiments where the iHESP-SOM is forced with the Q-flux forcings indicated in Figure 1 (left). For each WBC experiment, we conducted two sub-experiments with Q-flux forcings of opposite signs, specifically $+2\sigma$ and -2σ, where σ represents the winter monthly standard deviation in ocean heat flux convergence. The perturbation experiments were conducted by branching from each year of the iHESP-SOM control simulation to form 20-member ensembles for each region. For the Gulf stream and Kuroshio-Oyashio Extension forcings, the control simulation was branched on September 1st annually, applying the anomalous Q-flux forcing (plus control climatology) through March of the following year. For the Agulhas and Brazil-Malvinas experiments, the branching occurred on March 1st, with simulations running until the end of September. The last 6 months of the simulations were averaged for the analysis—October to March for the NH

and April to September for the SH. A two-sided student's *t*-test is employed to assess the statistical significance of the responses.

3. Results

The second through fourth columns of Figure 1; Figure S2 in Supporting Information S1 summarize key aspects of the iHESP-SOM response to the Q-flux forcings over all four WBCs. Again, the responses indicate the differences between the $+2\sigma$ and -2σ forcing runs and, overall, the turbulent heat fluxes and surface temperature closely mirror the forcing patterns. In all WBC regions, there are substantial increases in the surface latent heat fluxes and smaller increases in the surface sensible heat fluxes (Figure S2 in Supporting Information S1; the sign of the fluxes is positive upward). Also, the increases in the surface turbulent fluxes are accompanied by modest downstream decreases, which likely reflect the surface flux response to the resulting changes in the low-level atmospheric circulation (discussed below; see also Deser et al., 2010). The surface fluxes lead to a local warming of surface temperatures between 1 and 3°C (Figure 1, second column), with the warming generally extending further downstream than the forcings themselves. The Q-flux forcings have little effect on polar sea ice, except for modest ice melt to the northeast of the Antarctic Peninsula (Figure S2 in Supporting Information S1 right column), which underlies the poleward extension of the surface warming associated with the Brazil-Malvinas Confluence current system (Figure 1). Both the forcing and the responses are larger in the Gulf Stream and Kuroshio-Oyashio Extension than they are in the Agulhas and Brazil-Malvinas Confluence regions. As discussed below, the differences in the amplitudes of the forcings and surface temperature responses have implications for the large-scale circulation response.

The changes in the surface fluxes of heat are accompanied by changes in vertical motion at the top of the boundary layer, ∼850 hPa (Figure 1 third column). The most pronounced feature in the vertical motion response at 850 hPa is upward motion on the equatorward side of the maximum ocean surface warming (the maximum surface warming is indicated by the solid black lines), especially over the Gulf Stream and Kuroshio-Oyashio Extension. The upward anomalies are less clear over the SH WBCs: the Agulhas is marked by a zonally elongated band of upward motion on the equatorward side of the maximum heating, but the changes do not stand out relative to the noise in the response. The Brazil-Malvinas Confluence is associated with weak and spatially amorphous changes in vertical motion. There is enhanced downward motion on the poleward side of the region of largest heating over the Gulf Stream, but this feature is not as robust as the rising motion on the equatorward side. As shown below, the changes in vertical motion are clearer in vertical profiles of the response.

All four surface heating patterns are accompanied by robust increases in the model convective precipitation (Figure 1 right panel). Convective precipitation refers to the component of the precipitation field that is generated by the convective parameterization scheme, which simulates the precipitation originating from local air instability. This type of precipitation is typically associated with rapid updrafts that can lead to the formation of convective clouds and result in localized, intense rainfall events. As is the case for the vertical motion response, the most substantial increases in precipitation are found on the equatorward side of the region of largest surface heating. The responses are most pronounced over the Gulf Stream and Kuroshio-Oyashio Extension and are also clear over the Agulhas and Brazil-Malvinas Confluence current systems. The precipitation responses are consistent with results in Larson et al. (2024), who note substantial changes in precipitation associated with month-to-month variability in the SST field. Consistent with the influence of local surface heating on vertical motion, the responses are most clear in the convective component of the model precipitation and are not as readily apparent in the large-scale component of the precipitation field (not shown).

Figure 2 provides a vertically varying perspective of the vertical motion (left) and condensational heating (right) responses over all four WBCs. Results are averaged over the longitude ranges indicated by the green boxes in Figure 1, and then plotted as a function of latitude and height. The depth of the changes in vertical motion varies considerably from one WBC to the next (Figure 2 left panel). Over the Gulf Stream, significant upward motion extends from the lower troposphere to the tropopause throughout the latitude range 32–40°N. As also hinted at in the 850 hPa response in Figure 1, the upward motion over the Gulf Stream is paired with a weaker and shallower downward motion at 42–46°N. Similar changes in upward motion are found over the Kuroshio-Oyashio Extension, with notable upward motion anomalies found throughout much of the troposphere. The upward motion anomalies over the Kuroshio-Oyashio Extension have an interesting poleward tilt with height and decrease at a slightly lower upper tropospheric level than those over the Gulf Stream. In contrast to the responses

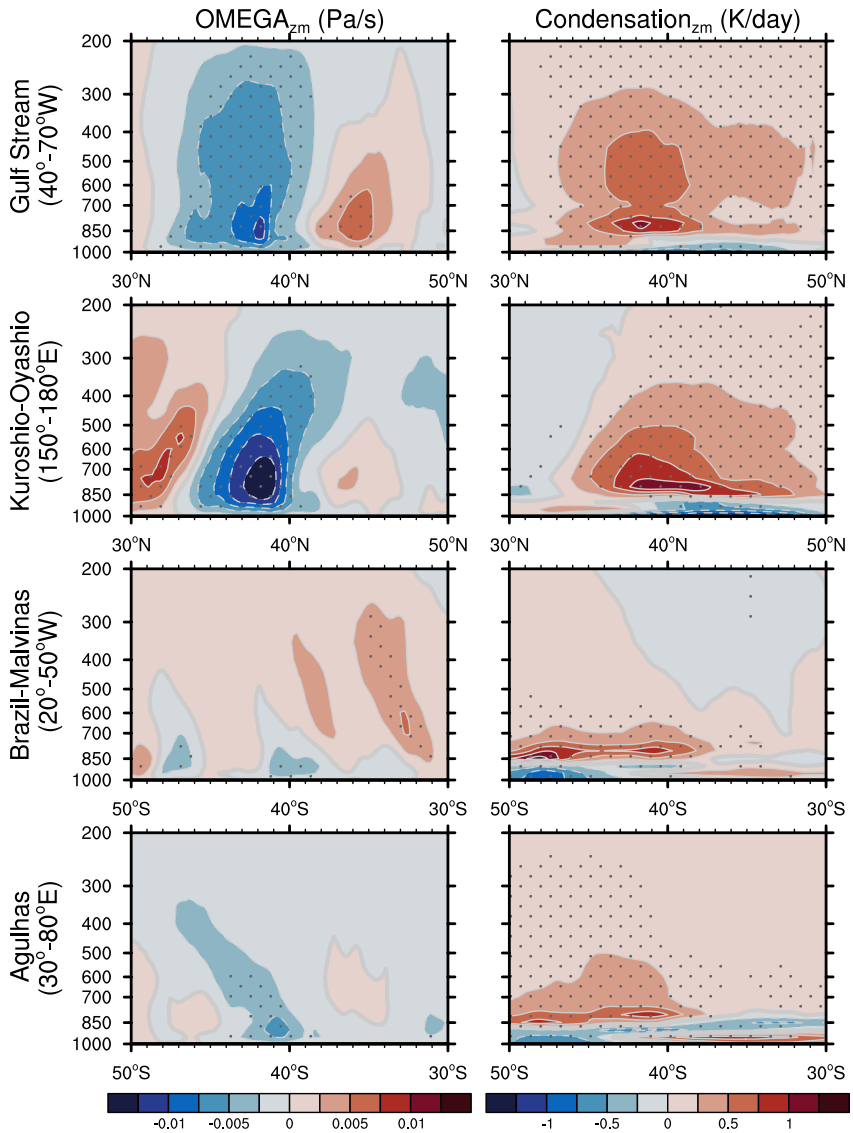

Figure 2. Responses of zonal-mean vertical motion (left panel shading; unit of Pa s^{-1}) and condensational heating (right panel; unit of K day^{-1}) to Q-flux forcings, averaged during the extended winter months across four major western boundary currents in both hemispheres. Stippled areas represent regions where results are statistically significant at the 95% level, determined by a two-sided student's *t*-test.

in the Gulf Stream and Kuroshio-Oyashio Extension, the vertical motion responses over the Agulhas and Brazil-Malvinas Confluence regions are weak and mostly confined to levels below ~850 hPa. The differences in the magnitude and vertical extent of the vertical motion response between the NH and SH WBCs are consistent with two key differences between the WBCs: (a) The Q-flux forcings over the SH WBCs are weaker than those applied to the NH WBCs; and (b) In observations, the climatological variance of vertical motion in the SH WBCs is much weaker than that over the NH WBCs (Figure S3 in Supporting Information S1).

The differences in the magnitude and depth of the vertical motion responses in the NH and SH WBCs are also reflected in the respective responses in condensational heating (Figure 2 right panel). Consistent with the changes in upward motion, the increases in condensational heating extend into the free troposphere over the Gulf Stream and Kuroshio-Oyashio Extension but are largely limited to levels below 700 hPa over the Agulhas and Brazil-Malvinas Confluence current systems. Hence, variations in ocean dynamical heating lead to changes in atmosphere heating that are restricted to the lower troposphere over the SH WBCs but extend well into the middle troposphere over the NH WBCs.

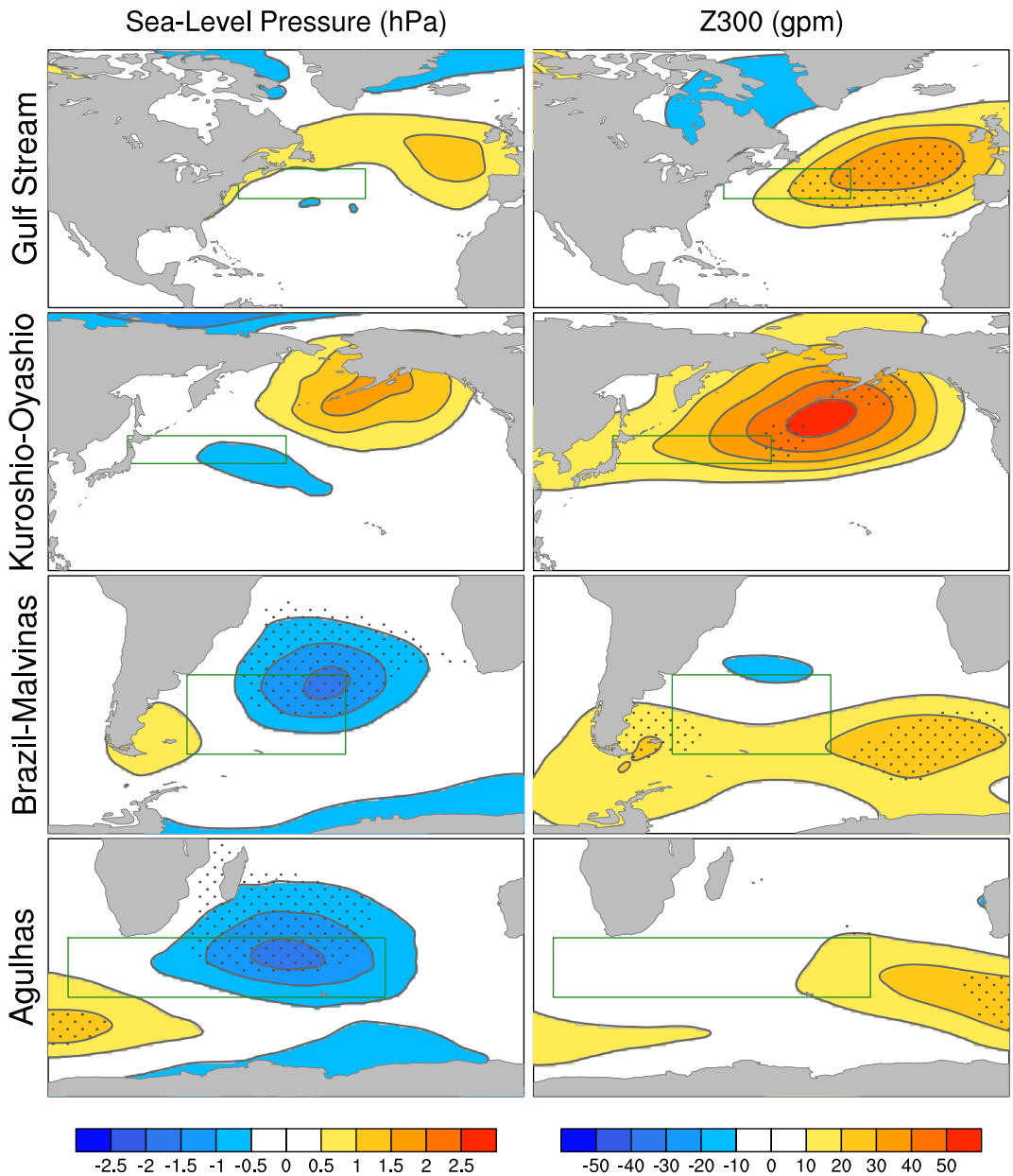

Figure 3. As in Figure 1, but for the responses of sea-level pressure (left panel; unit of hPa) and 300 hPa geopotential height (right panel; unit of gpm) to Q-flux forcings.

The differences between the vertical motion and condensational heating responses across the four WBCs have implications for the attendant changes in the large-scale atmospheric circulation. The atmospheric heating driven by the surface fluxes associated with anomalous ocean heat transport (i.e., Q-fluxes) can be balanced dynamically by either horizontal temperature advection or changes in vertical motion. If the heating is balanced by vertical motion, then it can lead to condensational heating and geopotential height anomalies that extend into the upper troposphere (Hoskins & Karoly, 1981; Smirnov et al., 2015). If the heating is balanced by low-level horizontal temperature advection, however, the atmospheric response may be largely limited to lower levels of the atmosphere, and will include decreases in lower tropospheric geopotential height that are shifted eastward of the forcing (Hoskins & Karoly, 1981). As shown in Figure 2, over the Gulf Stream and Kuroshio-Oyashio Extension, the heating is reflected in changes in vertical motion, convective precipitation, and condensational heating that extend through the depth of the troposphere. Consistent with the hydrostatic response to mid-tropospheric heating, there are notable increases in geopotential height aloft associated with the Q-flux forcings over both

NH WBCs (Figure 3, top two rows). The increases are shifted downstream of the surface forcing, which suggests the atmospheric condensational heating is shifted eastward by the atmospheric circulation. In contrast, over the Brazil-Malvinas Confluence and Agulhas regions, the changes in vertical motion and atmospheric heating are relatively shallow (Figure 2). Here the circulation response is dominated by surface low pressure that is shifted eastward of the Q-flux forcings and is thus consistent with northward flow and cold temperature advection over the surface heating (Figure 3, bottom two rows).

4. Summary and Discussion

The goal of this study was to investigate the influence of ocean heat transport over four major WBCs on vertical motion, precipitation, and the large-scale atmospheric circulation. To do so, we developed a slab-ocean version of a high-resolution climate model, and then forced the model with observed estimates of dynamical ocean heat transport over the Gulf Stream, Kuroshio-Oyashio Extension, Brazil-Malvinas Confluence, and Agulhas current systems. We then conducted ensemble experiments to explore the role of anomalous OHT on the atmospheric circulation. Specifically, we prescribed ocean heat flux convergence anomalies over four WBCs as a surface boundary condition in the iHESP-SOM. The ocean heat flux convergence anomalies were estimated from reanalysis products and thus reflect realistic forcing patterns that arise from OHT variability over four major WBCs, although to magnify the signals we have intentionally quadrupled the Q-flux forcing (i.e., 2σ minus -2σ). The key results include the following:

- Heating due to anomalous OHT over the Gulf Stream and Kuroshio-Oyashio Extension current systems leads to upward motion on the equatorward side of the maximum surface warming. The anomalous upward motion extends into the upper troposphere and is associated with notable changes in convective precipitation and condensational heating.
- Heating due to anomalous OHT over the Agulhas and Brazil-Malvinas Confluence current systems leads to robust changes in precipitation. But the changes in condensational heating and vertical motion are much shallower than those found in the NH current systems, and are largely limited to the levels below ~700 hPa.
- The differences in the depth of the vertical motion and condensational heating responses over the NH and SH WBCs lead to notable differences in the resulting changes in the large-scale atmospheric circulation. Over the Gulf Stream and Kuroshio-Oyashio Extension, the deep changes in condensational heating appear to be balanced by atmospheric vertical motion and are thus associated with robust changes in the upper tropospheric atmospheric circulation; over the Agulhas and Brazil-Malvinas Confluence current systems, the shallow changes in condensational heating appear to be balanced by horizontal temperature advection and the circulation response is thus most clear at low levels.

Why are the tropospheric responses to anomalous OHT over the Gulf Stream and Kuroshio-Oyashio Extension deeper and more pronounced than the responses to anomalous OHT over the Agulhas and Brazil-Malvinas Confluence current systems? There are several likely factors. One is that the magnitude of the Q-flux forcing is larger in the NH WBCs than it is in the SH WBCs. A second is that the observed variance in vertical motion is larger over the NH WBCs, which suggests the NH WBCs are marked by more pronounced coupling between the lower and upper troposphere. A third is that the vertical motion response may also be influenced by the latitudinal position of the Q-flux forcing relative to the jet stream. An observation-based study by Parfitt and Kwon (2020) indicated that the Gulf Stream's influence on the troposphere is largest when the eddy-driven jet is positioned further south and better aligned with the Gulf Stream. The Gulf Stream and Kuroshio-Oyashio Extension Q-flux forcings applied here are relatively close to the climatological-mean locations of the modeled Atlantic and Pacific jets, respectively. In contrast, the Agulhas and Brazil-Malvinas Confluence Q-flux forcings are situated much further from the SH eddy-driven jet. We plan to investigate the role of these various factors in the next step of our research. Moreover, this study focuses on the influence of large-scale OHT variability, rather than mesoscale ocean eddies, on atmospheric circulation. However, since the patterns of large-scale OHT anomalies prescribed in our experiments may be partly related to interactions operating at relatively small scales, the influence of small-scale oceanic processes on the atmospheric circulation is somewhat ambiguous based on our findings. Lastly, we note that our time-invariant Q-flux experiments capture only the atmospheric response to large-scale WBC variability. A time-varying Q-flux experiment, which would offer more insight into the effects of monthly WBC variability, is planned for future work.

Data Availability Statement

The ERA-5 reanalysis used in this study can be downloaded from the Research Data Archive (RDA) at European Centre For Medium-Range Weather Forecasts (2019). iHESP model data were obtained from the iHESP portal at https://ihesp.github.io/archive/. Post-processed data supporting our conclusions are available in the Zenodo data repository (Sun et al., 2024).

Acknowledgments

We appreciate the constructive suggestions of the two anonymous reviewers. Their comments improved the manuscript. We also acknowledge and are grateful for assistance from Dave Bailey and Nan Rosenbloom at NSF NCAR and discussions with James Larson at Colorado State University. We would like to acknowledge high-performance computing support from Cheyenne (https://doi.org/10.5065/D6RX99HX) provided by NCAR's Computational and Information Systems Laboratory, sponsored by the National Science Foundation. We acknowledge the support from the NSF CLD Program, under Grant AGS-2055121. DWJT is supported by the National Aeronautics and Space Administration (NASA) under 80NSSC23K0113 and the NSF CLD Program under AGS-2116186 and AGS-2055121.

References

Chang, P., Zhang, S., Danabasoglu, G., Yeager, S. G., Fu, H., Wang, H., et al. (2020). An unprecedented set of high-resolution Earth system simulations for understanding multiscale interactions in climate variability and change. *Journal of Advances in Modeling Earth Systems*, *12*, e2020MS002298. https://doi.org/10.1029/2020MS002298

Czaja, A., Frankignoul, C., Minobe, S., & Vannière, B. (2019). Simulating the midlatitude atmospheric circulation: What might we gain from high-resolution modeling of air-sea interactions? *Current Climate Change Reports*, *5*(4), 390–406. https://doi.org/10.1007/s40641-019-00148-5

Deser, C., Alexander, M. A., & Timlin, M. S. (2003). Understanding the persistence of sea surface temperature anomalies in midlatitudes. *Journal of Climate*, *16*(1), 57–72. https://doi.org/10.1175/1520-0442(2003)016<0057:utposs>2.0.co;2

Deser, C., Tomas, R. A., Alexander, M. A., & Lawrence, D. (2010). The seasonal atmospheric response to projected Arctic sea ice loss in the late twenty-first century. *Journal of Climate*, *23*(2), 333–351. https://doi.org/10.1175/2009JCLI3053.1

European Centre For Medium-Range Weather Forecasts. (2019). ERA5 reanalysis (monthly mean 0.25 degree latitude-longitude grid) [Dataset]. *UCAR/NCAR - Research Data Archive*. https://doi.org/10.5065/P8GT-0R61

Famooss Paolini, L., Athanasiadis, P. J., Ruggieri, P., & Bellucci, A. (2022). The atmospheric response to meridional shifts of the Gulf Stream SST front and its dependence on model resolution. *Journal of Climate*, *35*(18), 6007–6030. https://doi.org/10.1175/JCLI-D-21-0530.1

Frankignoul, C., Sennéchael, N., Kwon, Y., & Alexander, M. A. (2011). Influence of the meridional shifts of the Kuroshio and the Oyashio extensions on the atmospheric circulation. *Journal of Climate*, *24*(3), 762–777. https://doi.org/10.1175/2010JCLI3731.1

Hand, R., Keenlyside, N., Omrani, N. E., & Latif, M. (2014). Simulated response to inter-annual SST variations in the Gulf Stream region. *Climate Dynamics*, *42*(3–4), 715–731. https://doi.org/10.1007/s00382-013-1715-y

Hersbach, H., Bell, B., Berrisford, P., Hirahara, S., Horányi, A., Muñoz-Sabater, J., et al. (2020). The ERA5 global reanalysis. *Quarterly Journal of the Royal Meteorological Society*, *146*(730), 1999–2049. https://doi.org/10.1002/qj.3803

Hoskins, B. J., & Karoly, D. J. (1981). The steady linear response of a spherical atmosphere to thermal and orographic forcing. *Journal of the Atmospheric Sciences*, *38*(6), 1179–1196. https://doi.org/10.1175/1520-0469(1981)038,1179:TSLROA.2.0.CO;2

Huang, B., Liu, C., Banzon, V., Freeman, E., Graham, G., Hankins, B., et al. (2021). Improvements of the Daily Optimum Interpolation Sea Surface Temperature (DOISST) version 2.1. *Journal of Climate*, *34*(8), 2923–2939. https://doi.org/10.1175/JCLI-D-20-0166.1

Hurrell, J. W., Holland, M. M., Gent, P. R., Ghan, S., Kay, J. E., Kushner, P. J., et al. (2013). The Community Earth System Model: A framework for collaborative research. *Bulletin of the American Meteorological Society*, *94*(9), 1339–1360. https://doi.org/10.1175/BAMS-D-12-00121.1

Jia, Y., Chang, P., Szunyogh, I., Ramalingam, S., & Bacmeister, J. T. (2019). A modeling strategy for the investigation of the effect of mesoscale SST variability on atmospheric dynamics. *Geophysical Research Letters*, *46*(7), 3982–3989. https://doi.org/10.1029/2019GL081960

Joyce, T. M., Kwon, Y.-O., Seo, H., & Ummenhofer, C. C. (2019). Meridional Gulf Stream shifts can influence wintertime variability in the North Atlantic storm track and Greenland blocking. *Geophysical Research Letters*, *46*(3), 1702–1708. https://doi.org/10.1029/2018GL081087

Knutson, K. (2003). FMS slab ocean model technical documentation. Retrieved from https://www.gfdl.noaa.gov/fms-slab-ocean-model-technical-documentation/

Kobayashi, S., Ota, Y., Harada, Y., Ebita, A., Moriya, M., Onoda, H., et al. (2015). The JRA-55 reanalysis: General specifications and basic characteristics. *Journal of the Meteorological Society of Japan*, *93*(1), 5–48. https://doi.org/10.2151/jmsj.2015-001

Kushnir, Y., Robinson, W. A., Bladé, I., Hall, N. M. J., Peng, S., & Sutton, R. (2002). Atmospheric GCM response to extratropical SST anomalies: Synthesis and evaluation. *Journal of Climate*, *15*(16), 2233–2256. https://doi.org/10.1175/1520-0442(2002)015<2233:AGRTES>2.0.CO;2

Kwon, Y. O., Deser, C., & Cassou, C. (2011). Coupled atmosphere–mixed layer ocean response to ocean heat flux convergence along the Kuroshio Current Extension. *Climate Dynamics*, *36*(11–12), 2295–2312. https://doi.org/10.1007/s00382-010-0764-8

Larson, J. G., Thompson, D. W. J., & Hurrell, J. W. (2024). Signature of the western boundary currents in local climate variability. *Nature*, *634*(8035), 862–867. https://doi.org/10.1038/s41586-024-08019-2

Ma, X., Jing, Z., Chang, P., Liu, X., Montuoro, R., Small, R. J., et al. (2016). Western boundary currents regulated by interaction between ocean eddies and the atmosphere. *Nature*, *535*(7613), 533–537. https://doi.org/10.1038/nature18640

Ma, X., Nakamura, H., Montuoro, R., Wu, L., Wu, D., Chang, P., et al. (2016). Importance of resolving Kuroshio front and eddy influence in simulating the North Pacific storm track. *Journal of Climate*, *30*(5), 1861–1880. https://doi.org/10.1175/jcli-d-16-0154.1

Meehl, G. A., Yang, D., Arblaster, J. M., Bates, S. C., Rosenbloom, N., Neale, R., et al. (2019). Effects of model resolution, physics, and coupling on southern hemisphere storm tracks in CESM1.3. *Geophysical Research Letters*, *46*(21), 12408–12416. https://doi.org/10.1029/2019GL084057

Minobe, S., Small, R. J., Xie, S.-P., Komori, N., & Kuwano-Yoshida, A. (2008). Influence of the Gulf Stream on the troposphere. *Nature*, *452*(7184), 206–209. https://doi.org/10.1038/nature06690

Nakamura, H., Nishina, A., & Minobe, S. (2012). Response of storm tracks to bimodal Kuroshio path states south of Japan. *Journal of Climate*, *25*(21), 7772–7779. https://doi.org/10.1175/jcli-d-12-00326.1

Nakamura, H., Sampe, T., Goto, A., Ohfuchi, W., & Xie, S.-P. (2008). On the importance of midlatitude oceanic frontal zones for the mean state and dominant variability in the tropospheric circulation. *Geophysical Research Letters*, *35*(15), L15709. https://doi.org/10.1029/2008GL034010

Nkwinkwa Njouodo, A. S., Koseki, S., Keenlyside, N., & Rouault, M. (2018). Atmospheric signature of the Agulhas current. *Geophysical Research Letters*, *45*(10), 5185–5193. https://doi.org/10.1029/2018GL077042

O'Reilly, C. H., Minobe, S., Kuwano-Yoshida, A., & Woollings, T. (2017). The Gulf Stream influence on wintertime North Atlantic jet variability. *Quarterly Journal of the Royal Meteorological Society*, *143*, 173–183. https://doi.org/10.1002/qj.2907

Parfitt, R., Czaja, A., Minobe, S., & Kuwano-Yoshida, A. (2016). The atmospheric frontal response to SST perturbations in the Gulf Stream region. *Geophysical Research Letters*, *43*(5), 2299–2306. https://doi.org/10.1002/2016GL067723

Parfitt, R., & Kwon, Y. O. (2020). The modulation of Gulf Stream influence on the troposphere by the eddy-driven jet. *Journal of Climate*, *33*(10), 4109–4120. https://doi.org/10.1175/JCLI-D-19-0294.1

Patrizio, C. R., & Thompson, D. W. J. (2021). Quantifying the role of ocean dynamics in ocean mixed layer temperature variability. *Journal of Climate*, *34*(7), 2567–2589. https://doi.org/10.1175/JCLI-D-20-0476.1

Patrizio, C. R., & Thompson, D. W. J. (2022). Observed linkages between the atmospheric circulation and oceanic-forced sea-surface temperature variability in the western North Pacific. *Geophysical Research Letters*, *49*(8), e2021GL095172. https://doi.org/10.1029/2021GL095172

Peng, S., & Robinson, W. A. (2001). Relationships between atmospheric internal variability and the responses to an extratropical SST anomaly. *Journal of Climate*, *14*(13), 2943–2959. https://doi.org/10.1175/1520-0442(2001)014<2943:rbaiva>2.0.co;2

Peng, S., & Whitaker, J. S. (1999). Mechanisms determining the atmospheric response to midlatitude SST anomalies. *Journal of Climate*, *12*(5), 1393–1408. https://doi.org/10.1175/1520-0442(1999)012<1393:mdtart>2.0.co;2

Qiu, B., & Chen, S. (2010). Eddy-mean flow interaction in the decadally modulating Kuroshio Extension system. *Deep Sea Research Part II: Topical Studies in Oceanography*, *57*(13), 1098–1110. https://doi.org/10.1016/j.dsr2.2008.11.036

Reason, C. J. C. (2001). Evidence for the influence of the Agulhas current on regional atmospheric circulation patterns. *Journal of Climate*, *14*(12), 2769–2778. https://doi.org/10.1175/1520-0442(2001)014<2769:EFTIOT>2.0.CO;2

Seo, H., Kwon, Y., Joyce, T. M., & Ummenhofer, C. C. (2017). On the predominant nonlinear response of the extratropical atmosphere to meridional shifts of the Gulf Stream. *Journal of Climate*, *30*(23), 9679–9702. https://doi.org/10.1175/JCLI-D-16-0707.1

Siqueira, L., & Kirtman, B. P. (2016). Atlantic near-term climate variability and the role of a resolved Gulf Stream. *Geophysical Research Letters*, *43*(8), 3964–3972. https://doi.org/10.1002/2016GL068694

Small, R. J., Bryan, F. O., Bishop, S. P., & Tomas, R. A. (2019). Air–sea turbulent heat fluxes in climate models and observational analyses: What drives their variability? *Journal of Climate*, *32*(8), 2397–2421. https://doi.org/10.1175/JCLI-D-18-0576.1

Small, R. J., de Szoeke, S. P., Xie, S. P., O'Neill, L., Seo, H., Song, Q., et al. (2008). Air-sea interaction over ocean fronts and eddies. *Dynamics of Atmospheres and Oceans*, *45*(3–4), 274–319. https://doi.org/10.1016/j.dynatmoce.2008.01.001

Small, R. J., Msadek, R., Kwon, Y. O., Booth, J. F., & Zarzycki, C. (2019). Atmosphere surface storm track response to resolved ocean mesoscale in two sets of global climate model experiments. *Climate Dynamics*, *52*(3–4), 2067–2089. https://doi.org/10.1007/s00382-018-4237-9

Smirnov, D., Newman, M., Alexander, M. A., Kwon, Y., & Frankignoul, C. (2015). Investigating the local atmospheric response to a realistic shift in the Oyashio Sea surface temperature front. *Journal of Climate*, *28*(3), 1126–1147. https://doi.org/10.1175/JCLI-D-14-00285.1

Sun, L., Patrizio, C., Thompson, D., & Hurrell, J. (2024). Influence of extratropical ocean heat transport on atmospheric vertical motion variability in a high-resolution slab-ocean coupled model [Dataset]. *Zenodo*. https://doi.org/10.5281/zenodo.12548185

Sutton, R., & Mathieu, P.--P. (2002). Response of the atmosphere–ocean mixed-layer system to anomalous ocean heat-flux convergence. *Quarterly Journal of the Royal Meteorological Society*, *128*(582), 1259–1275. https://doi.org/10.1256/003590002320373283

Tomas, R. A., Deser, C., & Sun, L. (2016). The role of ocean heat transport in the global climate response to projected Arctic sea ice loss. *Journal of Climate*, *29*(19), 6841–6859. https://doi.org/10.1175/JCLI-D-15-0651.1

Tsujino, H., Urakawa, S., Nakano, H., Small, R. J., Kim, W. M., Yeager, S. G., et al. (2018). JRA-55 based surface dataset for driving ocean–sea-ice models (JRA55-do). *Ocean Modelling*, *130*, 79–139. https://doi.org/10.1016/j.ocemod.2018.07.002

Wills, R. C. J., Herrington, A. R., Simpson, I. R., & Battisti, D. S. (2024). Resolving weather fronts increases the large-scale circulation response to Gulf Stream SST anomalies in variable-resolution CESM2 simulations. *Journal of Advances in Modeling Earth Systems*, *16*(17), 1942–2466. https://doi.org/10.1029/2023MS004123

Yook, S., Thompson, D. W., Sun, L., & Patrizio, C. R. (2022). The simulated atmospheric response to western North Pacific sea-surface temperature anomalies. *Journal of Climate*, *35*(11), 1–43. https://doi.org/10.1175/JCLI-D-21-0371.1

Zhang, S., Fu, H., Wu, L., Li, Y., Wang, H., Zeng, Y., et al. (2020). Optimizing high-resolution community Earth system model on a heterogeneous many-core supercomputing platform. *Geoscientific Model Development*, *13*(10), 4809–4829. https://doi.org/10.5194/gmd-13-4809-2020